ACS APPLIED MATERIALS & INTERFACES

Research Article

Cite This: ACS Appl. Mater. Interfaces 2017, 9, 40151-40161

www.acsami.org

Layer-by-Layer Assembly of Polyoxometalates for Photoelectrochemical (PEC) Water Splitting: Toward Modular PEC Devices

Dasom Jeon,[†] Hyunwoo Kim,[†] Cheolmin Lee,[†] Yujin Han,[†] Minsu Gu,[†] Byeong-Su Kim,[†,‡] and Jungki Ryu*[,†]

[†]Department of Energy Engineering, School of Energy and Chemical Engineering, Ulsan National Institute of Science and Technology (UNIST), Ulsan 44919, Republic of Korea

[‡]Department of Chemistry, School of Natural Science, Ulsan National Institute of Science and Technology (UNIST), Ulsan 44919, Republic of Korea

Supporting Information

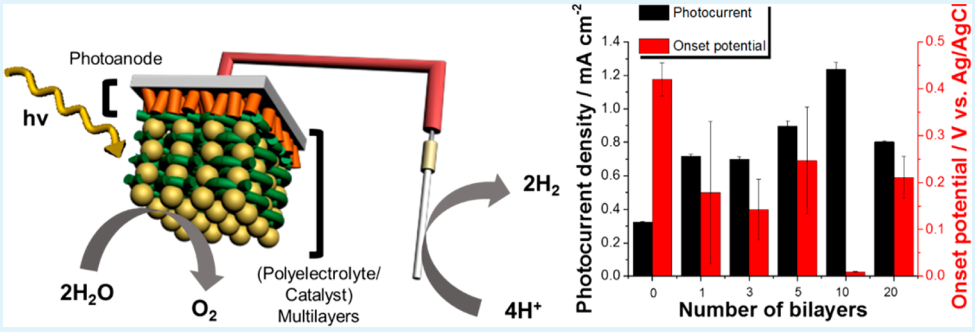

ABSTRACT: Artificial photosynthesis is considered one of the most promising solutions to modern energy and environmental crises. Considering that it is enabled by multiple components through a series of photoelectrochemical processes, the key to successful development of a photosynthetic device depends not only on the development of novel individual components but also on the rational design of an integrated photosynthetic device assembled from them. However, most studies have been dedicated to the development of individual components due to the lack of a general and simple method for the construction of the integrated device. In the present study, we report a versatile and simple method to prepare an efficient and stable photoelectrochemical device via controlled assembly and integration of functional components on the nanoscale using the layer-by-layer (LbL) assembly technique. As a proof of concept, we could successfully build a photoanode for solar water oxidation by depositing a thin film of diverse cationic polyelectrolytes and anionic polyoxometalate (molecular metal oxide) water oxidation catalysts on the surface of various photoelectrode materials (e.g., Fe_2O_3, $BiVO_4$, and TiO_2). It was found that the performance of photoanodes was significantly improved after the deposition in terms of stability as well as photocatalytic properties, regardless of types of photoelectrodes and polyelectrolytes employed. Considering the simplicity and versatile nature of LbL assembly techniques, our approach can contribute to the realization of artificial photosynthesis by enabling the design of novel photosynthetic devices.

KEYWORDS: *artificial photosynthesis, water splitting, photoelectrochemical cell, solar fuel, photocatalysis, layer-by-layer assembly, modular devices*

INTRODUCTION

Solar production of valuable chemicals, so-called artificial photosynthesis, has been a holey grail of scientists and engineers for decades as an alternative to conventional technologies for the production of fuels and raw chemicals.[1−7]

In principle, we can produce a variety of chemicals in a sustainable manner by rational design of photocatalytic systems with a proper combination and assembly of individual functional components.[1−5] For example, hydrogen gas can be photosynthesized from water in the presence of photosensitizers with an appropriate energy gap, hydrogen evolution catalysts, and water oxidation catalysts (WOCs) under visible light irradiation.[1,6] Recently, it has also been reported that carbon dioxide can be photocatalytically converted into useful raw chemicals such as carbon monoxide and formate for the synthesis of various chemical products.[2,7] Due to its huge potential and its environmental friendliness, various types of materials have been synthesized and evaluated to find better

Received: June 29, 2017
Accepted: November 3, 2017
Published: November 3, 2017

DOI: 10.1021/acsami.7b09416
ACS Appl. Mater. Interfaces 2017, 9, 40151−40161

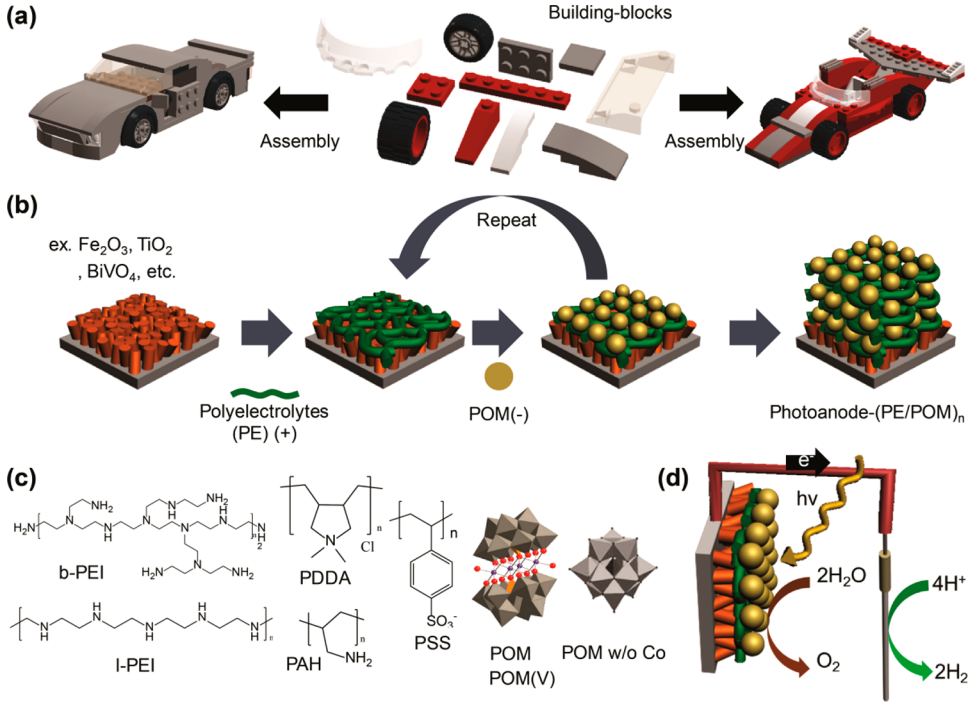

Figure 1. Layer-by-layer assembly (LbL) of a photoelectrochemical device can be compared to (a) the modular assembly of building blocks (i.e., functional components) into an integrated system (i.e., various types of devices). (b) The experimental procedure and (c) the molecular structure of the functional components used in this study is graphically illustrated. (d) Experimental setup for a photoelectrochemical water splitting to evaluate the photoelectrochemical performance of LbL-modified photoanodes prepared according to panel b.

components for artificial photosynthesis: light-harvesting materials[8,9] with a higher/broader absorbance and stability against degradation, reduction catalysts[10,11] with a lower overpotential and higher selectivity toward a specific product, and WOCs[12−29] with a lower overpotential and a higher stability against oxidation. There have also been reports about various types of photosynthetic systems: nanoparticulate photocatalysts loaded with cocatalysts,[10,30] Z-scheme devices,[31] wired[9,32]/wireless[6] photoelectrochemical cells, and hybrid devices[33] composed of a solar cell and an electrolysis cell.

However, most current studies have focused on the development and evaluation of new individual components without their integration into a photosynthetic device, only contributing to the broadening of the library of each component. Considering that a photosynthetic device is composed of various functional components, assembling them in a controllable and precise manner on the nanoscale are the key to the successful development of an efficient photosynthetic device (Figure 1a).[34,35] To enhance the performance of photoelectrodes, for example, researchers have tried to integrate various components (or building blocks) on their surface, such as protective layers,[5,15] charge separation/transporting materials,[36,37] and electrocatalysts[12−29] by various methods: electrodeposition,[9,25−27] vacuum deposition,[15,23,37] covalent immobilization,[10,24,29] and molecular recognition.[34,35] However, these methods can be applied only to a limited number of materials and often require special instruments and techniques for their implementation. Nevertheless, only a few efforts have been made to develop a universal method for the assembly of functional components in diverse combinations into an integrated photosynthetic device.

In the present study, we report a general and simple method to prepare an efficient and stable photoelectrochemical device via controlled assembly of organic and inorganic components using the layer-by-layer (LbL) deposition technique. We employed the LbL method, which has been rarely used to fabricate electrochemical[38] and photochemical devices,[29] because it allows the deposition of various materials with diverse sizes and shapes in various combinations without altering their properties through simple electrostatic interactions.[38−41] As a proof of concept, a photoanode for visible-light-driven water splitting was fabricated by the LbL method. We found that a model molecular water-oxidation catalyst (WOC), tetracobalt-substituted polyoxometalate (POM) anions can be readily integrated on various electrode surfaces such as α-Fe_2O_3, TiO_2, $BiVO_4$, fluorine-doped tin oxide (FTO), and gold by LbL assembly in the presence of cationic polyelectrolytes (PEs). After the deposition, the photoelectrochemical performance of photoanodes was significantly improved because of the synergistic effect of cationic PEs and anionic WOCs. Unexpectedly, the stability of photoanodes was also dramatically enhanced after the LbL modification due to the protective layer formed by cationic PEs. Considering the advantages of LbL assembly techniques, such as its simplicity and universal nature, the current study can present a step toward realization of artificial photosynthesis by providing a general and simple method for the construction of various electrochemical and photoelectrochemical systems.

RESULTS AND DISCUSSION

To demonstrate the validity of our approach for the development of an artificial photosynthetic device, we designed a series of experiments to construct various photoanodes (i.e., half-cell devices) for visible-light-driven water oxidation using the LbL method (Figure 1). Briefly, various substrates (e.g., α-Fe_2O_3, TiO_2, $BiVO_4$, gold, etc.) were sequentially treated with cationic PEs and anionic molecular WOCs for the desired

DOI: 10.1021/acsami.7b09416
ACS Appl. Mater. Interfaces 2017, 9, 40151−40161

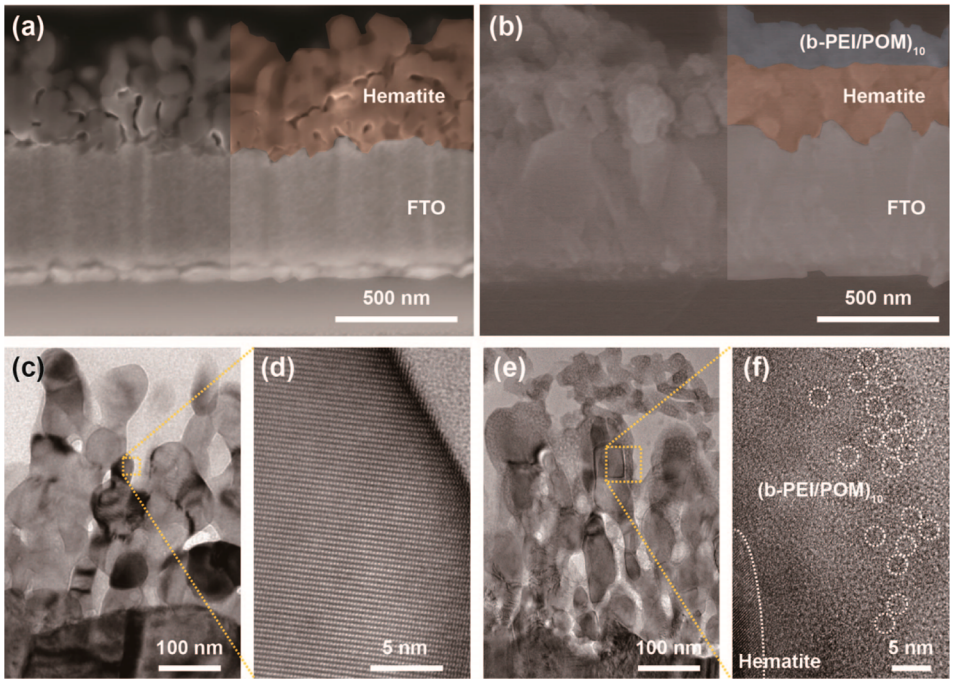

Figure 2. (a, b) SEM and (c–f) TEM micrographs of the hematite photoanode (a, c, d) before and (b, e, f) after the deposition of (b-PEI/POM)$_{10}$ bilayers. (a, b) Cross-sectional SEM images clearly show a morphological difference between the hematite photoanode (a) before and (b) after the deposition of (b-PEI/POM)$_{10}$ bilayers. Both original and false-colored SEM images are shown for comparison. (c–f) TEM images confirm the uniform and confomal deposition of the (b-PEI/POM)$_{10}$ bilayers on the hematite photoanode. Nanoscale dark spots with lattice fringe are highlighted with white dotted circles and thought to correspond to POMs.

number of times (Figure 1b). Here, we tested four different kinds of cationic PEs (Figure 1c and Table S1)—branched-poly(ethylenimine) (b-PEI), linear-poly(ethylenimine) (l-PEI), poly(allylamine hydrochloride) (PAH), and poly-(diallyldimethylammonium chloride) (PDDA)—for the integration of molecular WOCs onto a desired substrate. A tetracobalt-substituted polyoxometalate $[Co_4(H_2O)_2(PW_9O_{34})_2]^{10-}$ (POM) (Figure S1) was selected as a model WOC because it is well-known as an efficient hole scavenger and stable molecular WOC with multiple negative charges.[12,13] The performance of various photoanodes before and after the LbL modification was then evaluated by constructing a photoelectrochemical cell (Figure 1d) and measuring linear sweep voltammetry (LSV) and photocurrent density in the presence and absence of light irradiation. For convenience, A-(PE/POM)$_n$ indicates that an electrode A is modified with n number of bilayer films composed of cationic PEs and anionic POM catalysts.

First, we studied the effect of type of PE on the integration of POM WOCs onto a desired substrate by LbL assembly. Among various substrates, we initially tested α-Fe_2O_3 (hematite) because of its prominent advantages and disadvantages. Note that hematite is regarded as one of the most promising photoanode materials for solar water splitting due to its small bandgap and abundance.[8,25,32] However, there are many problems to be solved for its practical application, especially the ultrafast recombination of photogenerated holes and a large requisite overpotential for water splitting of ~0.5–0.6 V.[8] In this regard, hematite can be used as a model photoanode material to test the validity of our approach by modifying it with POM WOCs in various combinations by LbL assembly and then studying its photoelectrochemical properties. Tin-doped hematite film was readily prepared using the hydrothermal method according to the literature,[32] and its preparation was confirmed by X-ray diffraction (XRD) (Figure S2). The integration of molecular POM WOCs onto hematite surface using the LbL method was confirmed by scanning electron microscopy (SEM), transmission electron microscopy (TEM) and elemental analysis with X-ray photoelectron spectroscopy (XPS) and energy-dispersive X-ray spectroscopy. For example, top-view SEM micrographs showed a clear difference in the morphology of the hematite photoanode before (Figure S3a) and after (Figure S3b–d) the LbL modification with b-PEI and POM. After ten or more cycles of LbL assembly with b-PEI and POM, a thin layer of aggregates was coated on the entire electrode surface. Cross-sectional SEM and TEM analysis revealed that the LbL film was evenly and conformally deposited on the highly rugged hematite photoanode (Figure 2). While it is difficult to observe regular layered structures of the film, we could clearly observe uniform distribution of POMs in the LbL film without noticeable segregation (Figure 2e, f). The XPS (Figure S3e) and EDS (Figure S4) spectra showed that there is a relative increase of carbon (C)/nitrogen (N) and cobalt (Co)/phosphorus (P)/ tungsten (W) content after each LbL cycle, indicating the deposition of PEI and POM, respectively. The formation of (PE/POM) bilayers through the LbL assembly technique was also evidenced by in situ quartz crystal microbalance (QCM) analysis and ex situ spectroscopies. For in situ QCM analysis, a gold-coated quartz crystal disk was used instead of a hematite photoanode. We could observe the formation of (PE/POM) bilayers by monitoring the change of mass upon treatment with a PE and POM solution, regardless of the type of cationic PE employed (Figures S3f and S5). The formation of the LbL film was also investigated ex situ by UV–visible absorbance, Fourier transform infrared (FT-IR), and

DOI: 10.1021/acsami.7b09416
ACS Appl. Mater. Interfaces 2017, 9, 40151–40161

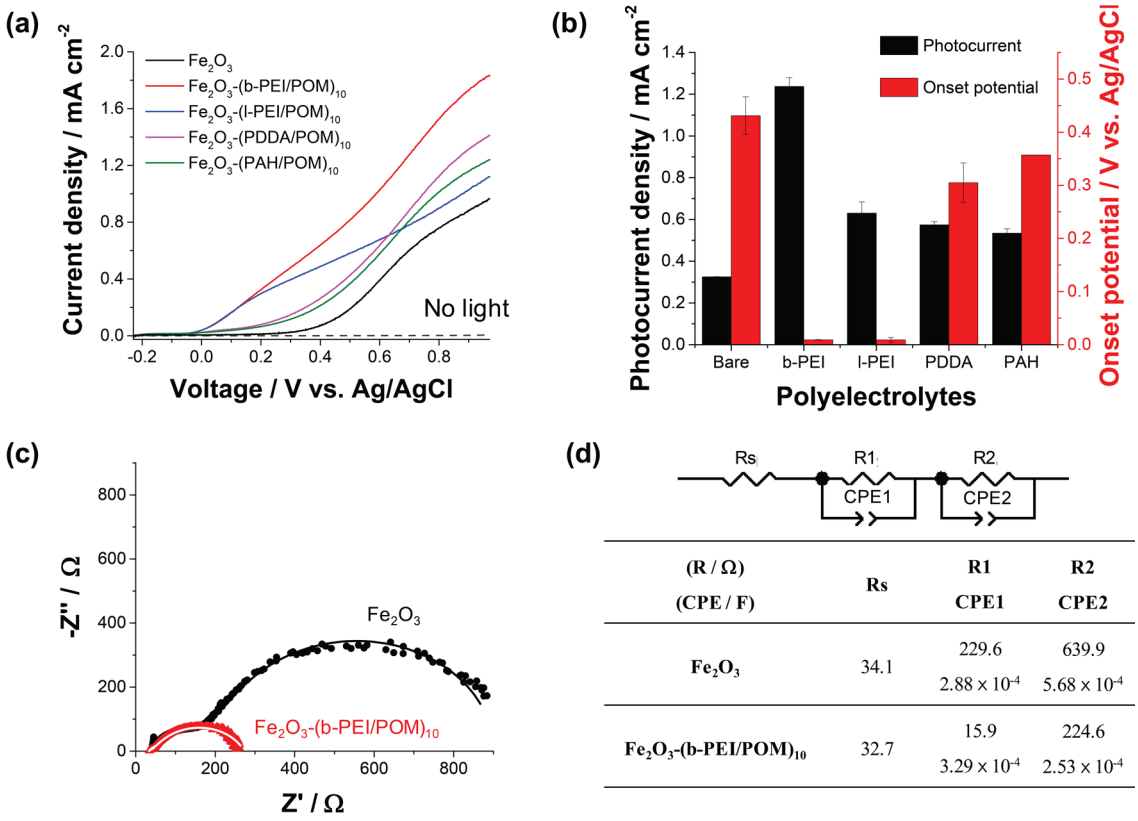

(R / Ω) (CPE / F)	Rs	R1 CPE1	R2 CPE2
Fe_2O_3	34.1	229.6 2.88×10^{-4}	639.9 5.68×10^{-4}
Fe_2O_3-(b-PEI/POM)$_{10}$	32.7	15.9 3.29×10^{-4}	224.6 2.53×10^{-4}

Figure 3. Influence of the LbL film composed of PE and POM WOCs on the photoelectrochemical of hematite photoanodes. The performance of different samples was compared by measuring (a) linear sweep voltammetry (LSV) and (b) summarized in terms of onset potential for water oxidation and photocurrent density with an applied bias of 0.6 V vs Ag/AgCl. (c, d) Electrochemical impedance spectra was measured, represented in the form of (c) the Nyquist plot, and (d) fitted using an equivalent circuit model.

Table 1. Comparison of the Photoelectrochemical Performance of Fe_2O_3 Photoanodes Modified by Various Methods

type of cocatalysts	onset potential shift (mV)	onset potential (mV vs RHE)	current density (mA cm^{-2})[a]	light source	electrolytes	scan rate (mV s^{-1})	modification methods	ref.
POM	410	0.68	0.94	300 W Xe 100 mW cm^{-2}	80 mM borate pH 8.0	20	layer-by-layer assembly	this study
Co-Pi	240	~1.0	<0.4	AM 1.5G 100 mW cm^{-2}	0.1 M phosphate and 0.2 M KCl, pH 6.9	5	photodeposition	16
IrO_x	300	~1.1	~0.2	450 W Xe 100 mW cm^{-2}	0.1 M phosphate pH 7.0		electrodeposition	17
Co_3O_4	40	0.66	1.2	150 W Xe 100 mW cm^{-2}	1 M NaOH		hydrothermal	18
Co-Pi	100	0.6	<0.6	AM 1.5G 100 mW cm^{-2}	1 M KOH and 0.2 M KCl	75	photoelectro-deposition	19
Co-Pi	170	0.9	2.8	AM 1.5G 100 mW cm^{-2}	1 M NaOH		photo-assisted electrodeposition	20
IrO_2	200	0.8	3	AM 1.5G 100 mW cm^{-2}	1 M NaOH	10	controlled potential electro-flocculation	21
$NiFeO_x$	380	0.62	<0.6	AM 1.5G 100 mW cm^{-2}	1 M NaOH		drop casting	22
NiOOH	160	0.58	1.64	AM 1.5G 100 mW cm^{-2}	1 M NaOH	20	photo-assisted electrodeposition	23
$Ni(OH)_2$	300	0.8	0.4	AM 1.5G 100 mW cm^{-2}	1 M KOH and 0.2 M KCl	20	atomic layer deposition	24
Ru complex	<100	0.9	~2	500 W Xe 100 mW cm^{-2}	1 M KOH	10	molecular immobilization	25

[a]Current density measured at 1.23 V vs RHE.

Raman spectroscopies (Figure S6). UV−visible spectra of the hematite photoanode showed a gradual increase of absorbance throughout the entire spectral region upon repetition of the LbL cycles. It might be due to the increased scattering of light by the formation and growth of a thin-layer of (b-PEI/POM) aggregates, which was also supported by FT-IR and Raman spectra.

On the basis of these results, we investigated the influence of type of cationic PE on the photoelectrochemical performance of the hematite photoanode modified with (PE/POM) bilayers.

DOI: 10.1021/acsami.7b09416
ACS Appl. Mater. Interfaces 2017, 9, 40151−40161

For comparison, the concentration of each PE for the LbL deposition was kept constant at 3 mM in terms of monomer concentration, and the number of (PE/POM) bilayers was fixed at ten for each sample. Since we used electrically and electrochemically inactive PEs for the integration of POM WOCs, one can expect that the performance of the photoanode remains unchanged or is even degraded after the LbL process. Interestingly, however, the performance of the hematite photoanode with (PE/POM) bilayers was significantly improved compared to bare hematite in terms of both onset potential for water oxidation and photocurrent density, regardless of the type of PE employed (Figures 3a, b and S7). Among the four different cationic PEs we tested, b-PEI was found to be most effective in terms of not only the amount of deposited POM (Figure S8) but also the performance of the photoanode after the modification. For comparison, hematite electrodes with ten bilayers of Co^{2+} cations and polystyrenesulfonate (PSS) by the LbL method and with the film of randomly mixed b-PEI and POM by drop-casting were prepared but exhibited a negligible catalytic activity (Figure S9), demonstrating that the improved performance is resulted from the precisely assembled structure as well as the integration of the POM WOCs. It is interesting to point out here that the columnar structure of the hematite and the LbL film is reminiscent of the mesoscale organization of thylakoid organelles[42] which ensures efficient transfer and utilization of electrons for photosynthesis.

Indeed, compared to the bare counterpart, Fe_2O_3-(b-PEI/POM)$_{10}$ exhibited outstanding performance with the largest cathodic shift of the onset potential by about 400 mV and a significant increase of photocurrent density (up to 0.94 mA cm^{-2}) by about three times with an applied bias of 1.23 V vs RHE (0.56 V vs Ag/AgCl at pH 8.0) under visible light irradiation. The performance improvement by the deposition of (PE/POM)$_{10}$ bilayers was even more pronounced at lower applied bias (Figure S10). Compared to previous reports,[16−25,43] the hematite electrode modified by the LbL method is found to have an excellent photoelectrochemical performance even at around neutral pH (Table 1). To the best of our knowledge, especially, the observed cathodic shift of the onset potential by about 400 mV is the largest among the reported to date for the hematite photoanode.[43] Note that a large cathodic shift of onset potential for water oxidation is highly beneficial to make a more efficient bias-free photoelectrochemical cell composed of a p-type photocathode and an n-type photoanode. It is because the maximum operating current of the cell can be estimated from the interception of the individually tested LSV curves of the photocathode and the photoanode, respectively (Figure S11).[5,32]

To elucidate the potential role of b-PEI on the improved photocatalytic activity of hematite photoanodes, we prepared four different kinds of hematite photoanodes by LbL assembly (Figure S12). These included bare Fe_2O_3, Fe_2O_3-(b-PEI/POM)$_{10}$, Fe_2O_3-(b-PEI/PSS)$_{10}$, and Fe_2O_3 with ten bilayers of b-PEI and polyoxometalates without a tetracobalt active site (Fe_2O_3-(b-PEI/POM w/o Co)$_{10}$) (Figure S12a). As shown in Figure S1, the POM without the active site ($(PW_9O_{34})^{9-}$) (POM w/o Co) alone has no catalytic activity at all. It was also found that polyelectrolytes alone (i.e., Fe_2O_3-(b-PEI/PSS)$_{10}$) have a negative effect on the performance of the hematite photoanode. Interestingly, the performance was significantly improved below a certain potential when these two components are assembled together (i.e., Fe_2O_3-(b-PEI/POM w/o CO)$_{10}$) (Figure S12b, c). This implies the synergistic effect of the LbL-assembled b-PEI and oxide clusters ($(PW_9O_{34})^{9-}$) on the performance of Fe_2O_3-(b-PEI/POM)$_{10}$. Recently, it is reported that polyoxometalates[44] and amine-containing molecules,[45] respectively, can act as a hole transporting layer for polymer-based optoelectronic devices, implying the potential role of the LbL assembled film in addition to the simple catalyst-loading effect.

To decouple factors that may affect the performance of the LbL-modified hematite electrodes, electrochemical impedance spectroscopy was carried out. All the impedance spectra are well fitted to a 2-RC-circuit model and consist of two semicircles (Figures 3c, d and S13 in the Supporting Information). The series resistance (R_S) including the substrate resistance, the resistance related to the ionic conductivity of an electrolyte solution, and external contact resistance was found to have a negligible difference between the samples. It could be easily expected that there is a decrease of the low-frequency charge transfer resistance (R_2) due to the improved electrocatalytic activity after the deposition of POM WOCs. Unexpectedly, we could also observe a significant decrease of the resistance at high frequencies (bigger than 100 Hz) (Figure S13), which can be related to the charge transport resistance (R_1)[46] in the Fe_2O_3 semiconductor. These results support the synergistic effect of the LbL-assembled layers of b-PEI and POMs on the performance improvement of the hematite photoanode. Considering that the LbL film might have a negligible effect on the bulk electrical properties (e.g., conductivity) of semiconductors and the charge transport resistance decreases as the strength of electric field increases in general,[46,47] it is thought that the alternating layers of cationic and anionic materials formed by the LbL assembly can act an interfacial dipole and contribute to the decrease of charge transport resistance. In principle, interfacial dipoles can induce the bending[48] of energy level and facilitate the charge transport in the semiconductor photoelectrode and to the POM WOCs. Our hypothesis can be also supported by a recent report[48] showing that the photocatalytic efficiency of semiconductors can be enhanced by introducing internal electric fields with ferroelectric materials.

As a next step, we tried to investigate the effect of the thickness or the number of the (b-PEI/POM) bilayers on the performance of the hematite photoanode. It was found that the photoelectrochemical performance of the hematite is gradually improved upon the deposition of up to ten bilayers and then degraded when more layers are deposited (Figures 4, S14a, and S15). However, hematite photoanodes modified by a large number of LbL bilayers (e.g., Fe_2O_3-(b-PEI/POM)$_{20}$) still show significantly improved performance compared to the bare one. Thus, it is thought that there is a critical thickness of the bilayer, below which photogenerated holes on hematite can be efficiently scavenged by POM WOCs for oxidation of water. Further studies are required to elucidate the underlying mechanism more in detail.

To exclude the possibility that the observed improvement in the performance of the hematite photoanode resulted from undesirable side reactions such as oxidation of PEs and photocorrosion of hematite, we carefully designed and conducted a set of experiments. First, we carried out cyclic voltammetry (CV) to study potential oxidation of amines in the presence and absence of POMs (Figure S16). The oxidation of b-PEI and water was readily distinguished in the cyclic voltammogram due to their different onset potentials. The

DOI: 10.1021/acsami.7b09416
ACS Appl. Mater. Interfaces 2017, 9, 40151−40161

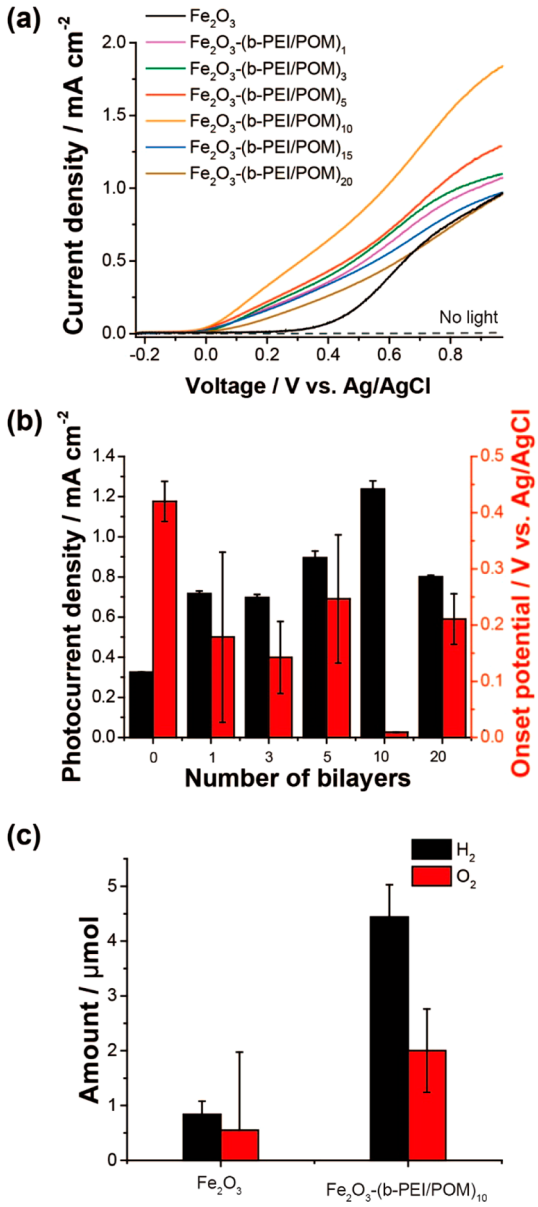

Figure 4. Effect of the number of (b-PEI/POM) bilayers on the photocatalytic performance of the hematite photoanode. The performance of different samples was compared by measuring (a) LSV and (b) summarized in terms of onset potential for water oxidation and photocurrent density. A three-electrode photoelectrochemical cell was prepared to quantify the total charge transfer by chronoamperogram (Figure S14) and (c) the actual amount of gas evolved by gas chromatography to calculate the Faradaic efficiency of the hematite electrode with and without (b-PEI/POM) bilayers.

onset potentials for oxidation of b-PEI and water were found to be around 0.7 and 1.0−1.1 V vs Ag/AgCl, respectively. Interestingly, it was found that the oxidation of b-PEI was significantly suppressed in the presence of POMs, possibly due to the fast hole-scavenging activity of POMs.[13] Second, we measured the Faradaic efficiency of the hematite photoanode for oxygen evolution before and after the LbL modification. The chronoamperogram of the hematite photoanode showed a gradual decrease of photocurrent density over time, but the overall tendency of the effect of the number of bilayers remained unchanged (Figure S14b). As expected from LSV and photocurrent measurement, the amount of oxygen and hydrogen evolved was significantly increased after the modification with (b-PEI/POM) bilayers (Figure 4c). The Faradaic efficiencies of the hematite photoanode before and after modification with $(b\text{-PEI/POM})_{10}$ bilayers were found to be 55 and 94%, respectively, with an applied bias of 0.77 V vs Ag/AgCl under visible light illumination at pH 8.0. For Fe_2O_3-$(b\text{-PEI/POM})_{10}$, the turnover number (TON) for oxygen evolution by POM was found to be 2.30×10^3 O_2/POM under the same condition. Taken together the results from CV analysis and the calculation of the Faradaic efficiency and the TON, we can conclude that the contribution of b-PEI oxidation to the performance improvement of the hematite photoanode was negligible after the LbL modification.

Since the low Faradaic efficiency of bare hematite implies the presence of unwanted side reactions such as photocorrosion of photoanodes,[49] we studied the morphology of the hematite photoanode before and after the photocatalytic water oxidation for 3 h. According to the literature[50] and the Pourbaix diagram[51] (Figure 5a), hematite exhibits poor stability at around neutral pHs due to cathodic corrosion. The bare hematite (Fe_2O_3) showed a clear morphological change after the reaction, such as fragmentation of hematite crystals possibly due to photocorrosion (Figure 5b). On the other hand, Fe_2O_3-$(b\text{-PEI/POM})_{10}$ exhibited a negligible morphological change after the reaction as expected from its high Faradaic efficiency (Figure 5b). Considering the cathodic corrosion of hematite at near-neutral pHs and the hole-scavenging activity of POMs, the observed stability improvement of the hematite photoanode is attributed to the formation of (b-PEI/POM) bilayers, especially b-PEI layers. The chronoamperometric measurement of photocurrent stability (Figure S14b) also indicates the high stability of the hematite electrode and the LbL film even at a high applied bias. It is interesting to point out here that b-PEI plays multiple vital roles in the improvement of the overall performance of hematite photoanodes: (1) an electrostatic adhesive for anionic POM WOCs, (2) an agent for improving charge transfer between hematite photoanodes and POM WOCs, and (3) a protective coating layer against the corrosion of hematite photoanodes.

Recently, there have been issues raised about the stability of POM WOCs.[52,53] In 2011, Finke et al.[52] reported that cobalt-based POM used in this study is not stable for the photoelectrochemical measurement and act as a raw material for CoO_x- or Co_3O_4-like WOCs. Although it is argued by Limberg et al.[53] which report the stability of POM on the basis of X-ray absorption spectroscopy (XAS), there still remain concerns about its stability. To address such concerns, we characterized the LbL-assembled hematite photoanode by Raman spectroscopy before and after measuring chronoamperogram with an applied bias of 0.77 V vs Ag/AgCl under visible light illumination for 3 h. As shown in Figure S17, there was a negligible change in Raman spectra after the test and no sign for the formation of CoO_x or Co_3O_4. To exclude the possibility of release of Co^{2+}, POM, and PEI from the LbL film, we also measured the UV/visible absorbance spectra of the electrolyte solution before and after the test and cannot find an evidence of dissolution or release of these species (Figure S18).

Lastly, to demonstrate the versatility of our approach for the substrate-independent assembly of various functional components for the construction of a photosynthetic device, we prepared various forms of photoanodes by the LbL modification of various materials such as Fe_2O_3, $BiVO_4$, and TiO_2. We first tried to deposit a different polyoxometalate

DOI: 10.1021/acsami.7b09416
ACS Appl. Mater. Interfaces 2017, 9, 40151−40161

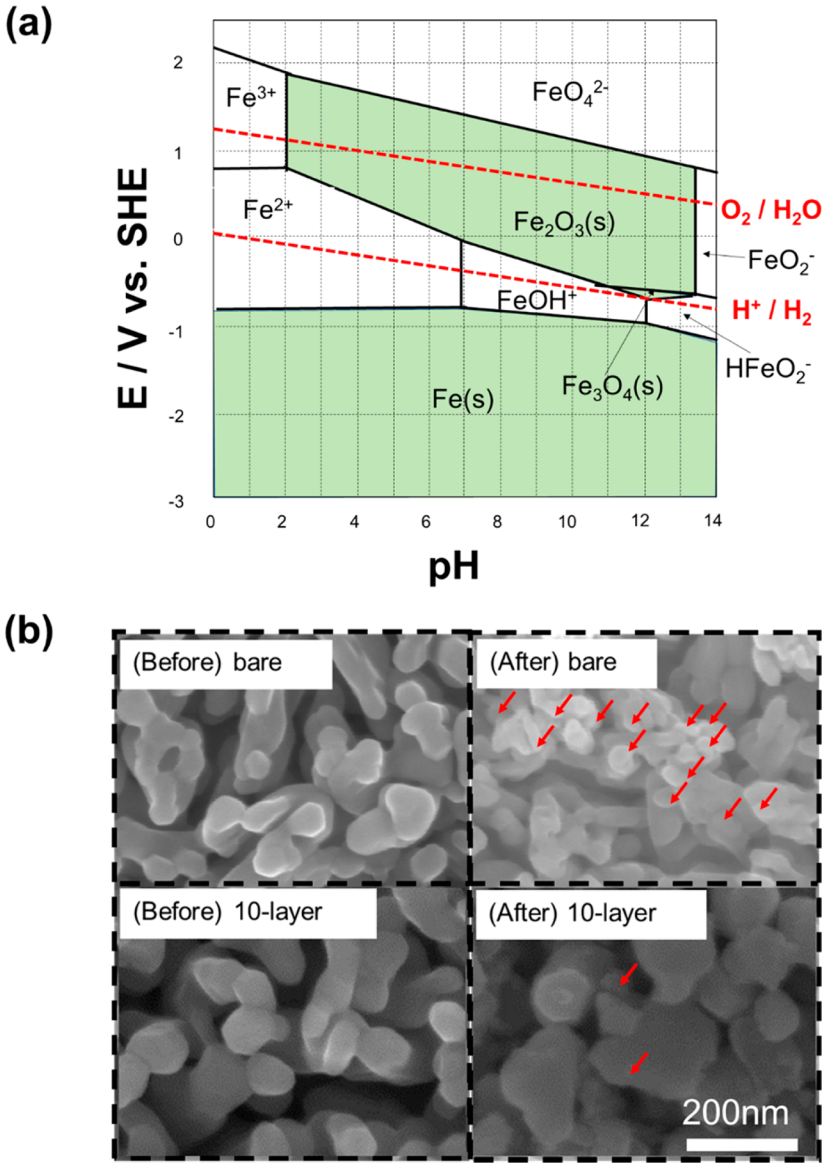

Figure 5. Stability of hematite photoanodes with and without $(b\text{-PEI/POM})_{10}$ bilayers. (a) The Pourbaix diagram for Fe−H_2O was obtained from the Materials Project database (http://www.materialsproject.org). (b) SEM micrographs of hematite with and without $(b\text{-PEI/POM})_{10}$ bilayers were compared before and after the photoelectrochemical test for 1 h with an applied bias of 0.6 V vs Ag/AgCl under visible light irradiation to study the effect of $(b\text{-PEI/POM})_{10}$ bilayers on the stability of hematite photoanodes.

WOC, $[Co_4(H_2O)_2(VW_9O_{34})_2]^{10-}$ (POM(V)),[14] which is structurally very similar to the POM we have used, $[Co_4(H_2O)_2(PW_9O_{34})_2]^{10-}$. Although POM(V) had a much higher electrocatalytic activity than POM, as shown in Figure S1, POM(V) was found to be less active when integrated on the hematite photoanode using the LbL method (Figure S19). This result indicates that the integration of WOCs with higher catalytic activity does not guarantee a higher overall performance of a photosynthetic device and that it is important to build and test an actual device in various combinations to find a better photosynthetic device. As a next step, we tried to integrate POM WOCs on different photoanode materials such as $BiVO_4$[9] and TiO_2,[1] which are also well-known as promising photoanode materials for solar water oxidation, and carefully examined their photocatalytic properties. They were synthesized according to the literature,[9,54] and their formation was confirmed by XRD (Figure S2). We could readily deposit multiple bilayers of b-PEI and POM WOCs on $BiVO_4$ (Figure 6a−c and Figure S20a, b) and TiO_2 (Figure 6d−f and Figure S20c, d), respectively, and successfully improve their photocatalytic properties in terms of onset potential and photocurrent density (Table S2).

Although here we only demonstrated the validity of our LbL-based approach for the construction of an oxidation half-reaction device with a few components, in principle, it can also be utilized to design and build various novel electrochemical (EC) and photoelectrochemical (PEC) devices. Contrary to conventional approaches relying on material-specific equipment and technique, our LbL-based approach can be applied to assemble diverse materials in various combinations and a desired order at nanoscale precision on any kind of substrate with complex geometries.[38−41] Despite these advantages, the LbL method has been rarely used in the fabrication of EC[38,55] and PEC devices because of concerns about incorporation of inactive components such as polyelectrolytes. In the present study, however, it was found that the incorporation of

DOI: 10.1021/acsami.7b09416
ACS Appl. Mater. Interfaces 2017, 9, 40151−40161

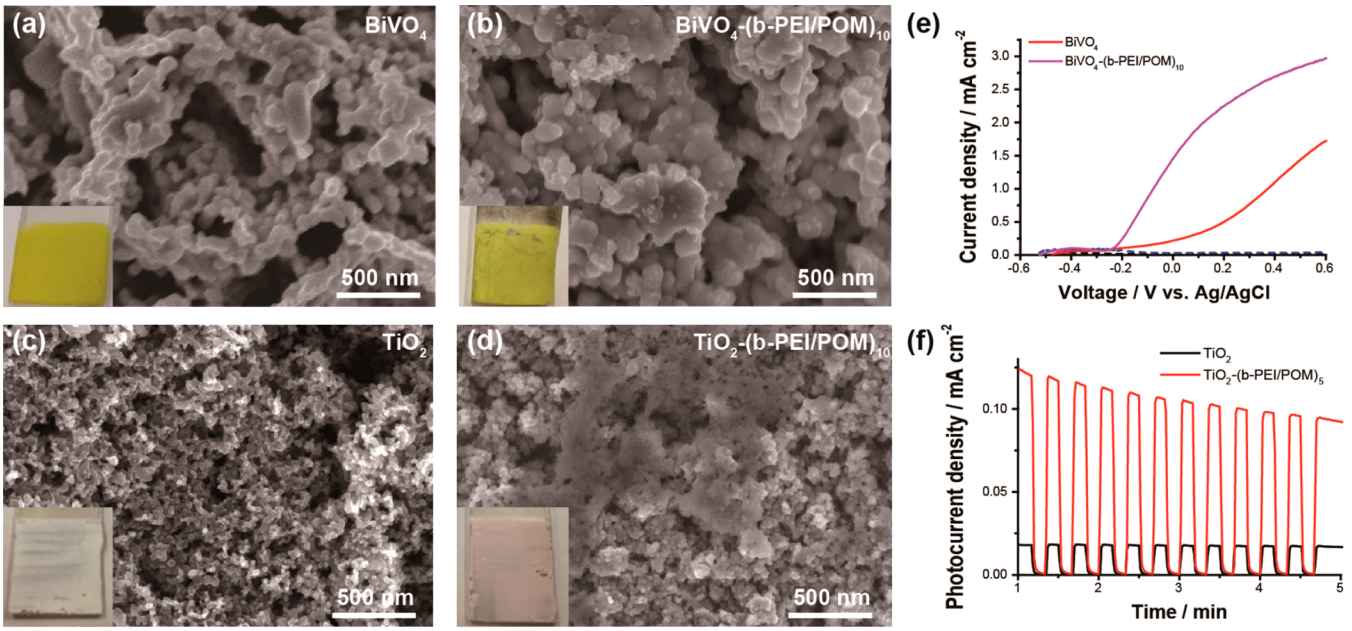

Figure 6. Improvement of the performance of (a–c) $BiVO_4$ and (d–f) TiO_2 photoanodes by layer-by-layer (LbL) assembly of cationic polyelectrolyte b-PEI and anionic POM water oxidation catalysts (WOCs). The formation of $(b\text{-PEI/POM})_n$ bilayers on $BiVO_4$ (n = 10) and TiO_2 (n = 5) photoanodes was confirmed by (a–d) electron microscopy, respectively, (a, c) before and (b, d) after the LbL treatment. Inset shows the corresponding photograph of the $BiVO_4$ and TiO_2 photoelectrodes on the FTO substrate, respectively. (e, f) The effect of the $(b\text{-PEI/POM})_n$ bilayers on the performance of (c) $BiVO_4$ and (f) TiO_2 photoanodes was studied by measuring LSV and photocurrent density with and without light irradiation. Note that visible and UV light was illuminated for $BiVO_4$ and TiO_2, respectively.

polyelectrolyte can contribute to the performance improvement of PEC devices by facilitating efficient charge transport and protecting photoelectrodes against corrosion or degradation. In this regard, we believe that our approach not only provides an alternative way to build a photosynthetic device, but also enables the design and realization of novel electrochemical and photoelectrochemical devices by providing higher degree of freedom in their design and fabrication.

CONCLUSION

To summarize, we report a versatile and simple, LbL-based method to assemble various functional components in the form of a photosynthetic device/system. As a proof of concept, we demonstrated that cationic PEs and anionic POM WOCs can be efficiently integrated on the surface of various photoelectrodes with complex geometries such as Fe_2O_3, $BiVO_4$, and TiO_2. It was found that their photoelectrochemical properties can be engineered by controlling various factors of LbL assembly such as types of PEs and the number of LbL bilayers. Furthermore, the LbL film was found to facilitate efficient charge transport and significantly improve the stability of photoelectrodes. Considering the versatile nature of LbL assembly for the deposition of multiple functional materials with diverse sizes and shapes in various combinations, it is thought that our LbL-based approach can not only provide a general and simple method for the controlled assembly of them to make an artificial photosynthetic device but also enable the designing of a novel electrochemical and photoelectrochemical system.

EXPERIMENTAL SECTION

Materials. All chemicals, unless otherwise stated, were purchased from Sigma-Aldrich (St. Louis, MO, USA). Poly(allylamine hydrochloride) and sodium nitrate was produced by Alfa Aesar (Ward Hill, MA, USA). The gold-coated quartz crystal disk was obtained from Stanford Research Systems (Sunnyvale, CA, USA).

Fabrication of Various Photoanodes. Hematite photoanodes were prepared by a simple hydrothermal method according to the literature.[32] Briefly, a clean FTO substrate was prepared, loaded in a 50 mL Teflon-lined stainless steel autoclave containing a 10 mL aqueous solution of 0.15 M $FeCl_3$ and 1.0 M $NaNO_3$, and treated at 100 °C for 1 h to grow FeOOH film. Tin-doped hematite film was prepared by annealing the FeOOH film on FTO at 800 °C in air for 5 min. The overall process was repeated one more time. Nanoporous TiO_2 photoanodes were fabricated by using a doctor-blade method. Briefly, TiO_2 paste was prepared by ultrasonically mixing 1 g of commercially available TiO_2 nanoparticles with 10 mL of ethanol for 30 min and adding 3% of titanium isopropoxide to the mixture under vigorous stirring. TiO_2 paste was then casted on ITO by the doctor-blade method and annealed at 150 °C for 1 h to obtain nanoporous TiO_2 film. $BiVO_4$ photoanodes were obtained by electrochemical deposition of BiOI film on FTO and its chemical conversion to $BiVO_4$, according to the literature.[9] A precursor solution for electrodeposition of BiOI was prepared by dissolving 0.04 M $Bi(NO_3)_3$ in 50 mL of 0.4 M KI solution, adjusting the pH of the solution to 1.7 with HNO_3, and then mixing with 20 mL of 0.23 M p-benzoquinone solution in ethanol. The electrodeposition of BiOI was carried out with a WMPG1000 multichannel potentiostat/galvanostat (WonATech Co. Ltd., Korea) under the following conditions: working electrode, FTO glass; reference electrode, Ag/AgCl; counter electrode, Pt wire; applied potential, −0.1 V vs Ag/AgCl. The BiOI electrode was converted to $BiVO_4$ by treating it in the presence of 0.2 M vanadyl acetylacetonate at 400 °C with a ramping rate of 2 °C/min and selectively removing unwanted V_2O_5 with 1 M NaOH solution.

Synthesis of Polyoxometalate-Based Water Oxidation Catalysts. A tetracobalt-substituted polyoxometalate (POM) water oxidation catalyst (WOC), $[Co_4(H_2O)_2(PW_9O_{34})_2]^{10-}$, was synthesized according to the literature.[12] Briefly, the sodium salt of POM was produced by preparing a neutral aqueous solution of 1.08 M $Na_2WO_4 \cdot 2H_2O$, 0.12 M Na_2HPO_4, 0.24 M $Co(NO_3)_2 \cdot 6H_2O$ and refluxing it at 100 °C for 2 h. The resultant POM WOCs were purified by recrystallization.

DOI: 10.1021/acsami.7b09416
ACS Appl. Mater. Interfaces 2017, 9, 40151–40161

Deposition of (Polyelectrolyte−POM)$_n$ Bilayers on Various Substrates by LbL Assembly Technique. For the integration of negatively charged POM catalysts by LbL assembly technique, we used four different cationic polyelectrolytes: branched-poly(ethylene imine) (b-PEI), linear-poly(ethylene imine) (l-PEI), poly(allylamine hydrochloride) (PAH), and poly(diallyldimethylammonium chloride) (PDDA). For LbL assembly, cationic polyelectrolytes and anionic POMs were dissolved at 3 mM (in terms of monomer concentration) and 1 mM, respectively, in a 10 mM phosphate buffer with 137 mM of NaCl (pH 5.0). One cycle of LbL assembly consists of sequential treatment of the substrate with polyelectrolyte and POM solutions for 5 min each. The substrate was washed with deionized water for 30 s three times between each cycle and treated repeatedly for the desired number of times.

Characterization. Morphology and elemental composition of samples were characterized by an S-4800 scanning electron microscope (SEM) (Hitachi High-Technologies, Japan) equipped with an energy dispersive X-ray spectrometer (EDS). The formation of (polyelectrolyte/POM) bilayers on various electrodes was confirmed with multiple analytical tools such as a V-730 UV−visible spectrophotometer (JASCO, Japan), a Cary 670/620 Fourier transform infrared (FT-IR) microscope (Agilent Technologies, Santa Clara, CA, USA), an alpha 300R confocal Raman microscope (WITec, German), and a QCM200 quartz crystal microbalance (QCM) (Stanford Research Systems, Sunnyvale, CA, USA).

Photoelectrochemical Characterization. The photoelectrochemical performance of photoelectrodes was characterized by linear sweep voltammetry (LSV) in the presence and absence of visible light irradiation with a WMPG1000 multichannel potentiostat/galvanostat under the following conditions: working electrode, photoelectrodes with and without the LbL modification; reference electrode, Ag/AgCl; counter electrode, Pt wire; electrolyte, 80 mM phosphate buffer (PB, pH 8.0); visible light source, 300W Xe lamp equipped with a 400 nm cut-on filter. Evolution of oxygen and hydrogen gas during the photoelectrochemical test was identified and quantified with a GC-2010 Plus gas chromatograph (Shimadzu Co., Japan). All measurements were done at least in triplicate for statistical analysis. Electrochemical impedance spectra were measured using a 1260 impedance analyzer from Solartron under the following conditions: reference electrode, Ag/AgCl; counter electrode, Pt wire; electrolyte, 80 mM phosphate buffer (pH 8.0); applied potential of 0.5 V vs Ag/AgCl; amplitude, 10 mV; frequency scan range, 100 kHz to 0.1 Hz. The Faradaic efficiency was calculated by dividing the number of electrons used for water oxidation and that flown through a photoelectrochemical cell, assuming four-electron oxidation of water. Turnover number was calculated from the ratio between the total number of oxygen produced and POM deposited, which were determined by gas chromatography and QCM analysis, respectively.

■ ASSOCIATED CONTENT

Supporting Information

The Supporting Information is available free of charge on the ACS Publications website at DOI: 10.1021/acsami.7b09416.

Table summarizing the properties of the polyelectrolytes used in this study; cyclic voltammogram of different polyoxometalates; X-ray diffraction patterns of various photoanodes; SEM micrographs, XPS/EDS spectra, QCM analysis, and optical spectra showing the deposition of the LbL layers on photoanode; chronoamperogram showing the photocatalytic activity of the hematite electrode with the LbL layers; quantification of the deposited polyelectrolytes and POM WOCs by the LbL method; LSV curves for various forms of photoanodes; influence of types of cationic polyelectrolytes on the performance of the hematite photoanode as a function of the applied bias; plot showing the importance of a large cathodic shift of the onset potential; magnified Nyquist plot; chronoamperogram showing the effect of the number of bilayers on the performance; cyclic voltammogram of b-PEI in the presence and absence of POMs; Raman spectra of Fe_2O_3-(b-PEI/POM)$_{10}$ before and after the PEC test; absorbance spectra showing the stability of the LbL film; table summarizing the enhancement of PEC performance of $BiVO_4$ and TiO_2 photoanodes by the LbL deposition (PDF)

■ AUTHOR INFORMATION

Corresponding Author

*E-mail: jryu@unist.ac.kr.

ORCID

Dasom Jeon: 0000-0002-2297-0396
Hyunwoo Kim: 0000-0002-1550-9745
Cheolmin Lee: 0000-0001-6740-2782
Yujin Han: 0000-0003-1240-2720
Minsu Gu: 0000-0002-6270-7496
Byeong-Su Kim: 0000-0002-6419-3054
Jungki Ryu: 0000-0002-0897-8463

Notes

The authors declare no competing financial interest.

■ ACKNOWLEDGMENTS

This work was supported by Basic Science Research Program (NRF-2015R1C1A1A02037698) and Nano-Material Technology Development Program (NRF-2017M3A7B4052802) through the National Research Foundation of Korea (NRF) funded by the Ministry of Science, ICT, & Future Planning of Korea and by the Brain Korea 21 Plus program through NRF funded by the Ministry of Education of Korea. This work was also supported by the 2015 Research Fund (1.150092.01) of UNIST (Ulsan National Institute of Science and Technology).

■ REFERENCES

(1) Chen, X.; Shen, S.; Guo, L.; Mao, S. S. Semiconductor-Based Photocatalytic Hydrogen Generation. *Chem. Rev.* **2010**, *110*, 6503−6570.

(2) Kim, D.; Sakimoto, K. K.; Hong, D.; Yang, P. Artificial Photosynthesis for Sustainable Fuel and Chemical Production. *Angew. Chem., Int. Ed.* **2015**, *54*, 3259−3266.

(3) Ryu, J.; Lee, S. H.; Nam, D. H.; Park, C. B. Rational Design and Engineering of Quantum-Dot-Sensitized TiO_2 Nanotube Arrays for Artificial Photosynthesis. *Adv. Mater.* **2011**, *23*, 1883−1888.

(4) Ryu, J.; Nam, D. H.; Lee, S. H.; Park, C. B. Biocatalytic Photosynthesis with Water as an Electron Donor. *Chem. - Eur. J.* **2014**, *20*, 12020−12025.

(5) Sun, K.; Shen, S.; Liang, Y.; Burrows, P. E.; Mao, S. S.; Wang, D. Enabling Silicon for Solar-Fuel Production. *Chem. Rev.* **2014**, *114*, 8662−8719.

(6) Reece, S. Y.; Hamel, J. A.; Sung, K.; Jarvi, T. D.; Esswein, A. J.; Pijpers, J. J. H.; Nocera, D. G. Wireless Solar Water Splitting Using Silicon-Based Semiconductors and Earth-Abundant Catalysts. *Science* **2011**, *334*, 645−648.

(7) White, J. L.; Baruch, M. F.; Pander, J. E., III; Hu, Y.; Fortmeyer, I. C.; Park, J. E.; Zhang, T.; Liao, K.; Gu, J.; Yan, Y.; Shaw, T. W.; Abelev, E.; Bocarsly, A. B. Light-Driven Heterogeneous Reduction of Carbon Dioxide: Photocatalysts and Photoelectrodes. *Chem. Rev.* **2015**, *115*, 12888−12935.

(8) Sivula, K.; Le Formal, F.; Gratzel, M. Solar Water Splitting: Progress using Hematite α-Fe_2O_3 Photoelectrodes. *ChemSusChem* **2011**, *4*, 432−449.

DOI: 10.1021/acsami.7b09416
ACS Appl. Mater. Interfaces 2017, 9, 40151−40161

(9) Kim, T. W.; Choi, K. S. Nanoporous $BiVO_4$ Photoanodes with Dual-Layer Oxygen Evolution Catalysts for Solar Water Splitting. *Science* **2014**, *343*, 990−994.
(10) Muresan, N. M.; Willkomm, J.; Mersch, D.; Vaynzof, Y.; Reisner, E. Immobilization of a Molecular Cobaloxime Catalyst for Hydrogen Evolution on a Mesoporous Metal Oxide Electrode. *Angew. Chem., Int. Ed.* **2012**, *51*, 12749−12753.
(11) Laursen, A. B.; Kegnæs, S.; Dahl, S.; Chorkendorff, I. Molybdenum Sulfides—Efficient and Viable Materials for Electro - and Photoelectrocatalytic Hydrogen Evolution. *Energy Environ. Sci.* **2012**, *5*, 5577−5591.
(12) Yin, Q.; Tan, J. M.; Besson, C.; Geletii, Y. V.; Musaev, D. G.; Kuznetsov, A. E.; Luo, Z.; Hardcastle, K. I.; Hill, C. L. A Fast Soluble Carbon-Free Molecular Water Oxidation Catalyst Based on Abundant Metals. *Science* **2010**, *328*, 342−345.
(13) Orlandi, M.; Argazzi, R.; Sartorel, A.; Carraro, M.; Scorrano, G.; Bonchio, M.; Scandola, F. Ruthenium Polyoxometalate Water Splitting Catalyst: Very Fast Hole Scavenging from Photogenerated Oxidants. *Chem. Commun.* **2010**, *46*, 3152−3154.
(14) Lv, H.; Song, J.; Geletii, Y. V.; Vickers, J. W.; Sumliner, J. M.; Musaev, D. G.; Kogerler, P.; Zhuk, P. F.; Bacsa, J.; Zhu, G.; Hill, C. L. An Exceptionally Fast Homogeneous Carbon-Free Cobalt-Based Water Oxidation Catalyst. *J. Am. Chem. Soc.* **2014**, *136*, 9268−9271.
(15) Sun, K.; Saadi, F. H.; Lichterman, M. F.; Hale, W. G.; Wang, H. P.; Zhou, X.; Plymale, N. T.; Omelchenko, S. T.; He, J. H.; Papadantonakis, K. M.; Brunschwig, B. S.; Lewis, N. S. Stable Solar-Driven Oxidation of Water by Semiconducting Photoanodes Protected by Transparent Catalytic Nickel Oxide Films. *Proc. Natl. Acad. Sci. U. S. A.* **2015**, *112*, 3612−3617.
(16) Klahr, B.; Gimenez, S.; Fabregat-Santiago, F.; Bisquert, J.; Hamann, T. W. Photoelectrochemical and Impedance Spectroscopic Investigation of Water Oxidation with "Co-Pi"-Coated Hematite Electrodes. *J. Am. Chem. Soc.* **2012**, *134*, 16693−16700.
(17) Badia-Bou, L.; Mas-Marza, E.; Rodenas, P.; Barea, E. M.; Fabregat-Santiago, F.; Gimenez, S.; Peris, E.; Bisquert, J. Water Oxidation at Hematite Photoelectrodes with an Iridium-Based Catalyst. *J. Phys. Chem. C* **2013**, *117*, 3826−3833.
(18) Xi, L. F.; Tran, P. D.; Chiam, S. Y.; Bassi, P. S.; Mak, W. F.; Mulmudi, H. K.; Batabyal, S. K.; Barber, J.; Loo, J. S. C.; Wong, L. H. Co_3O_4-Decorated Hematite Nanorods As an Effective Photoanode for Solar Water Oxidation. *J. Phys. Chem. C* **2012**, *116*, 13884−13889.
(19) Zandi, O.; Hamann, T. W. Enhanced Water Splitting Efficiency Through Selective Surface State Removal. *J. Phys. Chem. Lett.* **2014**, *5*, 1522−1526.
(20) Zhong, D. K.; Cornuz, M.; Sivula, K.; Grätzel, M.; Gamelin, D. R. Photo-Assisted Electrodeposition of Cobalt−Phosphate (Co−Pi) Catalyst on Hematite Photoanodes for Solar Water Oxidation. *Energy Environ. Sci.* **2011**, *4*, 1759−1764.
(21) Du, C.; Yang, X.; Mayer, M. T.; Hoyt, H.; Xie, J.; McMahon, G.; Bischoping, G.; Wang, D. Hematite-Based Water Splitting with Low Turn-On Voltages. *Angew. Chem., Int. Ed.* **2013**, *52*, 12692−12695.
(22) Tamirat, A. G.; Su, W.-N.; Dubale, A. A.; Chen, H.-M.; Hwang, B.-J. Photoelectrochemical Water Splitting at Low Applied Potential Using a NiOOH Coated Codoped (Sn, Zr) α-Fe_2O_3 Photoanode. *J. Mater. Chem. A* **2015**, *3*, 5949−5961.
(23) Young, K. M.; Hamann, T. W. Enhanced Photocatalytic Water Oxidation Efficiency with $Ni(OH)_2$ Catalysts Deposited on α-Fe_2O_3 via ALD. *Chem. Commun.* **2014**, *50*, 8727−8730.
(24) Fan, K.; Li, F.; Wang, L.; Daniel, Q.; Chen, H.; Gabrielsson, E.; Sun, J.; Sun, L. Immobilization of a Molecular Ruthenium Catalyst on Hematite Nanorod Arrays for Water Oxidation with Stable Photocurrent. *ChemSusChem* **2015**, *8*, 3242−3247.
(25) Tilley, S. D.; Cornuz, M.; Sivula, K.; Gratzel, M. Light-Induced Water Splitting with Hematite: Improved Nanostructure and Iridium Oxide Catalysis. *Angew. Chem., Int. Ed.* **2010**, *49*, 6405−6408.
(26) Kanan, M. W.; Nocera, D. G. Situ Formation of an Oxygen-Evolving Catalyst in Neutral Water Containing Phosphate and Co^{2+}. *Science* **2008**, *321*, 1072−1075.
(27) Carroll, G. M.; Zhong, D. K.; Gamelin, D. R. Mechanistic Insights into Solar Water Oxidation by Cobalt-Phosphate-Modified α-Fe_2O_3 Photoanodes. *Energy Environ. Sci.* **2015**, *8*, 577−584.
(28) Jiao, F.; Frei, H. Nanostructured Cobalt Oxide Clusters in Mesoporous Silica as Efficient Oxygen-Evolving Catalysts. *Angew. Chem., Int. Ed.* **2009**, *48*, 1841−1844.
(29) Lauinger, S. M.; Sumliner, J. M.; Yin, Q.; Xu, Z.; Liang, G.; Glass, E. N.; Lian, T.; Hill, C. L. High Stability of Immobilized Polyoxometalates on TiO_2 Nanoparticles and Nanoporous Films for Robust, Light-Induced Water Oxidation. *Chem. Mater.* **2015**, *27*, 5886−5891.
(30) Maeda, K.; Domen, K. Development of Novel Photocatalyst and Cocatalyst Materials for Water Splitting under Visible Light. *Bull. Chem. Soc. Jpn.* **2016**, *89*, 627−648.
(31) Maeda, K.; Higashi, M.; Lu, D. L.; Abe, R.; Domen, K. Efficient Nonsacrificial Water Splitting through Two-Step Photoexcitation by Visible Light using a Modified Oxynitride as a Hydrogen Evolution Photocatalyst. *J. Am. Chem. Soc.* **2010**, *132*, 5858−5868.
(32) Jang, J. W.; Du, C.; Ye, Y.; Lin, Y.; Yao, X.; Thorne, J.; Liu, E.; McMahon, G.; Zhu, J.; Javey, A.; Guo, J.; Wang, D. Enabling unassisted solar water splitting by iron oxide and silicon. *Nat. Commun.* **2015**, *6*, 7447.
(33) Luo, J. S.; Im, J. H.; Mayer, M. T.; Schreier, M.; Nazeeruddin, M. K.; Park, N. G.; Tilley, S. D.; Fan, H. J.; Gratzel, M. Water Photolysis at 12.3% Efficiency via Perovskite Photovoltaics and Earth-Abundant Catalysts. *Science* **2014**, *345*, 1593−1596.
(34) Vilona, D.; Di Lorenzo, R.; Carraro, M.; Licini, G.; Trainotti, L.; Bonchio, M. Viral Nano-Hybrids for Innovative Energy Conversion and Storage Schemes. *J. Mater. Chem. B* **2015**, *3*, 6718−6730.
(35) Nam, Y. S.; Magyar, A. P.; Lee, D.; Kim, J. W.; Yun, D. S.; Park, H.; Pollom, T. S., Jr.; Weitz, D. A.; Belcher, A. M. Biologically Templated Photocatalytic Nanostructures for Sustained Light-Driven Water Oxidation. *Nat. Nanotechnol.* **2010**, *5*, 340−344.
(36) Maeda, K.; Xiong, A.; Yoshinaga, T.; Ikeda, T.; Sakamoto, N.; Hisatomi, T.; Takashima, M.; Lu, D.; Kanehara, M.; Setoyama, T.; Teranishi, T.; Domen, K. Photocatalytic Overall Water Splitting Promoted by Two Different Cocatalysts for Hydrogen and Oxygen Evolution under Visible Light. *Angew. Chem., Int. Ed.* **2010**, *49*, 4096−4099.
(37) Yang, X.; Liu, R.; Du, C.; Dai, P.; Zheng, Z.; Wang, D. Improving Hematite-Based Photoelectrochemical Water Splitting with Ultrathin TiO_2 by Atomic Layer Deposition. *ACS Appl. Mater. Interfaces* **2014**, *6*, 12005−12011.
(38) Choi, Y.; Gu, M.; Park, J.; Song, H. K.; Kim, B. S. Graphene Multilayer Supported Gold Nanoparticles for Efficient Electrocatalysts Toward Methanol Oxidation. *Adv. Energy. Mater.* **2012**, *2*, 1510−1518.
(39) Xiao, F. X.; Pagliaro, M.; Xu, Y. J.; Liu, B. Layer-by-Layer Assembly of Versatile Nanoarchitectures with Diverse Dimensionality: A New Perspective for Rational Construction of Multilayer Assemblies. *Chem. Soc. Rev.* **2016**, *45*, 3088−3121.
(40) Lee, T.; Min, S. H.; Gu, M.; Jung, Y. K.; Lee, W.; Lee, J. U.; Seong, D. G.; Kim, B.-S. Layer-by-Layer Assembly for Graphene-Based Multilayer Nanocomposites: Synthesis and Applications. *Chem. Mater.* **2015**, *27*, 3785−3796.
(41) Richardson, J. J.; Cui, J.; Bjornmalm, M.; Braunger, J. A.; Ejima, H.; Caruso, F. Innovation in Layer-by-Layer Assembly. *Chem. Rev.* **2016**, *116*, 14828−14867.
(42) Ferreira, K. N.; Iverson, T. M.; Maghlaoui, K.; Barber, J.; Iwata, S. Architecture of the Photosynthetic Oxygen-Evolving Center. *Science* **2004**, *303*, 1831−1838.
(43) Tamirat, A. G.; Rick, J.; Dubale, A. A.; Su, W.-N.; Hwang, B.-J. Using Hematite for Photoelectrochemical Water Splitting: A Review of Current Progress and Challenges. *Nanoscale Horiz.* **2016**, *1*, 243−267.
(44) Vasilopoulou, M.; Polydorou, E.; Douvas, A. M.; Palilis, L. C.; Kennou, S.; Argitis, P. Annealing-Free Highly Crystalline Solution-Processed Molecular Metal Oxides for Efficient Single-Junction and Tandem Polymer Solar Cells. *Energy Environ. Sci.* **2015**, *8*, 2448−2463.
(45) Lee, B. R.; Lee, S.; Park, J. H.; Jung, E. D.; Yu, J. C.; Nam, Y. S.; Heo, J.; Kim, J. Y.; Kim, B. S.; Song, M. H. Amine-Based Interfacial

DOI: 10.1021/acsami.7b09416
ACS Appl. Mater. Interfaces 2017, 9, 40151−40161

Molecules for Inverted Polymer-Based Optoelectronic Devices. *Adv. Mater.* **2015**, *27*, 3553−3559.
(46) Lopes, T.; Andrade, L.; Le Formal, F.; Gratzel, M.; Sivula, K.; Mendes, A. Hematite Photoelectrodes for Water Splitting: Evaluation of the Role of Film Thickness by Impedance Spectroscopy. *Phys. Chem. Chem. Phys.* **2014**, *16*, 16515−16123.
(47) Le Formal, F.; Tétreault, N.; Cornuz, M.; Moehl, T.; Grätzel, M.; Sivula, K. Passivating Surface States on Water Splitting Hematite Photoanodes with Alumina Overlayers. *Chem. Sci.* **2011**, *2*, 737−743.
(48) Li, L.; Salvador, P. A.; Rohrer, G. S. Photocatalysts with Internal Electric Fields. *Nanoscale* **2014**, *6*, 24−42.
(49) Chen, Z.; Dinh, H. N.; Miller, E. *Photoelectrochemical Water Splitting: Standards, Experimental Methods, and Protocols*. Springer: New York, 2013; p x, 126 p.
(50) Kim, J. Y.; Jang, J. W.; Youn, D. H.; Magesh, G.; Lee, J. S. A Stable and Efficient Hematite Photoanode in a Neutral Electrolyte for Solar Water Splitting: Towards Stability Engineering. *Adv. Energy. Mater.* **2014**, *4*, 1400476.
(51) Li, Z. S.; Luo, W. J.; Zhang, M. L.; Feng, J. Y.; Zou, Z. G. Photoelectrochemical Cells for Solar Hydrogen Production: Current State of Promising Photoelectrodes, Methods to Improve Their Properties, and Outlook. *Energy Environ. Sci.* **2013**, *6*, 347−370.
(52) Stracke, J. J.; Finke, R. G. Electrocatalytic Water Oxidation Beginning with the Cobalt Polyoxometalate $[Co_4(H_2O)_2(PW_9O34)_2]^{10-}$: Identification of Heterogeneous CoO_x as the Dominant Catalyst. *J. Am. Chem. Soc.* **2011**, *133*, 14872−14875.
(53) Schiwon, R.; Klingan, K.; Dau, H.; Limberg, C. Shining Light on Integrity of a Tetracobalt-Polyoxometalate Water Oxidation Catalyst by X-Ray Spectroscopy before and after Catalysis. *Chem. Commun.* **2014**, *50*, 100−102.
(54) Hoang, T. T.; Nguyen, P. H.; Huynh, T. P.; Nguyen, T. V. Enhanced Charge Transfer of Liquid and Gel Electrolytes Using Nano Platinum in Dye-sensitized Solar Cells. *IEEE Phot. Spec. Conf.* **2013**, 2713−2715.
(55) Pappa, A. M.; Inal, S.; Roy, K.; Zhang, Y.; Pitsalidis, C.; Hama, A.; Pas, J.; Malliaras, G. G.; Owens, R. M. Polyelectrolyte Layer-by-Layer Assembly on Organic Electrochemical Transistors. *ACS Appl. Mater. Interfaces* **2017**, *9*, 10427−10434.

DOI: 10.1021/acsami.7b09416
ACS Appl. Mater. Interfaces 2017, 9, 40151−40161